

THE SPECTROSCOPY OF PLASMA EVOLUTION FROM ASTROPHYSICAL RADIATION MISSION

J. EDELSTEIN¹, K. W. MIN², W. HAN³, E. J. KORPELA¹,
K. NISHIKIDA¹, B.Y. WELSH¹, C. HEILES¹, J. ADOLFO¹, M. BOWEN¹, W.M. FEUERSTEIN¹, K. MCKEE¹,
J.-T. LIM², K. RYU², J.-H. SHINN², U.-W. NAM³, J.-H. PARK³, I.-S. YUK³, H. JIN³, K.I SEON³, D.H. LEE³, E. SIM⁴

¹Space Sciences Laboratory, University of California, Berkeley, CA 94720

²Korea Advanced Institute of Science and Technology, 305-701, Daejeon, Korea

³Korea Astronomy and Space Science Institute, 305-348, Daejeon, Korea and

⁴Korea Aerospace Research Institute, 305-333, Daejeon, Korea

Draft version July 14, 2018

ABSTRACT

The Spectroscopy of Plasma Evolution from Astrophysical Radiation (or the Far-ultraviolet Imaging Spectrograph) instruments, flown aboard the STSAT-1 satellite mission, have provided the first large-area spectral mapping of the cosmic far ultraviolet (FUV, λ 900-1750) background. We observe diffuse radiation from hot ($10^4 - 10^6$ K) and ionized plasmas, molecular hydrogen, and dust scattered starlight. These data provide for the unprecedented detection and discovery of spectral emission from a variety of interstellar environments, including the general medium, molecular clouds, supernova remnants, and super-bubbles. We describe the mission and its data, present an overview of the diffuse FUV sky's appearance and spectrum, and introduce the scientific findings detailed later in this volume.

Subject headings: ultraviolet: ISM: general

1. INTRODUCTION

The Spectroscopy of Plasma Evolution from Astrophysical Radiation instruments (hereafter *SPEAR*, also known as the Far-ultraviolet Imaging Spectrograph or *FIMS*) have provided the first large-area spectral sky survey of cosmic far ultraviolet (FUV) radiation. The FUV band (λ 900-1750) includes important astrophysical diagnostics such as strong atomic cooling lines from hot ($T=10^4$ K - 10^6 K) and photoionized plasmas as well as radiation from molecular hydrogen (H_2) fluorescent emission and dust scattered starlight. We describe the *SPEAR* mission and its science motivation, introduce the data by presenting the spatial distribution of the FUV (λ 1360 -1710) sky brightness and the spectra of the entire observed sky, and provide a brief introduction to other *SPEAR* science results described in the accompanying papers in this Volume.

SPEAR is the primary payload on the STSAT-1 (S-1) satellite launched 2003 September 27. The mission has thus far observed $\sim 80\%$ of the sky and conducted deep pointed observations toward numerous selected targets. *SPEAR* contains dual imaging spectrographs optimized for the measurement of diffuse FUV emission. The spectrographs, referred to as the Short wavelength band 'S' ($\lambda\lambda$ 900 - 1150, $4.0^\circ \times 4.6'$ view) and Long wavelength band 'L': $\lambda\lambda$ 1350 - 1750, $7.4^\circ \times 4.3'$ view), each have a spectral resolution of $\lambda/\Delta\lambda \sim 550$ half-energy width and an imaging resolution of $5'$. Each instrument uses a collecting mirror, a diffraction grating and an open faced, photon counting micro-channel plate detector. The *SPEAR* instruments, their on-orbit performance, and the basic processing of instrument data are described in detail in the following paper (Edelstein et al. *ibid.*).

2. ENERGETIC PLASMA IN THE ISM

Supernovae and stellar winds produce shock-heated gas in the Galaxy. The activity powered by the energetic plasma shapes the structure of the Galaxy, effecting

the distribution of metals and driving evolutionary phenomena such as star formation that depend on global morphology. On smaller scales, hot gas can power a variety of radiative, mechanical and chemical phenomena by forming turbulent and evaporative structures, altering chemical abundance via dust ablation or vaporizing dust condensates, and by radiatively influencing the gas ionization balance. Candidate mechanisms (see McKee (1995) for an overview) by which interstellar plasmas cool include (1) energy exchange with surrounding media such as evaporation and conduction, (2) mechanical cooling such as adiabatic expansion, (3) direct emissive radiation, and (4) indirect radiation by way of heated dust-grain emission. Our understanding of shock-ISM interactions and the global structure of ionized gas in our Galaxy are far from complete. Several models for the origin of this hot ionized gas have been proposed (Slavin & Cox 1992, 1993; Shapiro & Benjamin 1991; Borkowski et al. 1990; Shelton 1998) that make distinctive, verifiable predictions, yet none can be ruled out with current observations.

Very hot interstellar diffuse gas ($T \geq 10^6$ K) was first mapped by *ROSAT* soft X-ray (SXR) background observations (Snowden et al. 1998) which show pervasive regions of SXR gas at high latitudes, conceivably caused by hot gas injected into the Galactic halo, although uncertainty remains regarding the state of this gas. A component of this SXR emission has been attributed to local hot gas but charge-exchange between the Solar wind and the heliospheric environs may confuse the observations by producing the same detected species (Lallement 2004; Wargelin et al. 2004). Sanders et al. (2001) and McCammon et al. (2002) have recorded SXR diffuse emission spectra that are inconsistent with predictions of standard models of hot ionized gas but these data may also be contaminated by Solar charge exchange. The *CHIPS* mission (Hurwitz et al. 2005) EUV observations have established upper limits to local hot gas that are an order of magnitude less than expected from the

postulated local SXR emitting gas, unless this plasma is extremely depleted. (EUV observations are limited by interstellar absorption to nearby regions, with $N(\text{HI}) < 10^{18.5} \text{ cm}^{-2}$.)

An overwhelming fraction ($> 85\%$) of the radiative cooling power from hot, thin interstellar plasma is emitted in the FUV (Landini & Monsignori Fossi 1990). These FUV transitions, from the most abundant atoms in prevalent ground states, provide important diagnostics for both collisional and photoionized species. FUV absorption observations have revealed the hot ionized Galactic ISM. Measurements taken with *IUE* and *HST* have shown that Si IV, C IV, and N V ions, characteristic of $T = 10^{4.5}-10^6 \text{ K}$ gas, exist throughout the Galaxy with scale heights up to 4–5 kpc (Sembach & Savage 1992). Hotter gas, with $T=10^{5.2}-10^6 \text{ K}$ and indicated by O VI $\lambda\lambda 1032$ absorption, has been observed with *Copernicus*, *Voyager*, *ORFEUS*, *HUT* and now *FUSE* (Jenkins 1978; Hurwitz et al. 1995; Davidsen 1993; Zsargó et al. 2003). The O VI appears ubiquitous, although patchy in distribution, and perhaps extends to several kpc scale height (Savage et al. 2003). FUV absorption measurements, limited to sight lines with suitable background sources, cannot alone yield the physical state parameters of the hot plasma (e.g. n_e , T , pressure, filling factor) and are not suited to the detection of lines from gas with a large velocity dispersion because placement of the adjacent stellar continuum is problematic.

Detection of FUV interstellar emission lines from the ISM has proven to be difficult. Measurements with sounding rocket experiments, short-lived orbital missions and small instruments on interplanetary missions have suffered from inadequate spectral or spatial resolution; an inability to carefully correct for noise sources such as intense geocoronal emission, bright stars and dust-scattered stellar continuum; or from integration periods insufficient to obtain sensitive results. (See Bowyer (1991) for a review of earlier work.) Space observatories with FUV measurement capability (e.g., *Copernicus*, *IUE*, *HUT*, *ORFEUS*, *GHRs*, *STIS*, *FUSE*) have been optimized for point source observations and not for measuring faint diffuse spectra over the large angular scales needed to characterize the Galactic plasma. Although the *GALEX* mission (Martin et al. 2005) was designed to observe large areas of the sky, it has a limited capacity for mapping Galactic diffuse emission and must exclude observations of regions including bright stars. *GALEX* records either a broad-band image including no spectral information, or an objective-dispersion image that obtains low resolution spectra of localized sources but can confuse diffuse sources with angular extent.

Despite these difficulties, the detection of interstellar C IV and O III] FUV line emission was reported (Martin & Bowyer 1990) 15 years ago (and not since, until now). These lines were observed at intensities of several thousand LU^1 toward four locations, from which the properties of an interstellar component were derived, with $n_e = 0.01 - 0.02 \text{ cm}^{-3}$ and $T = 10^{4.7}-10^{5.3} \text{ K}$ (Shull & Slavin 1994). Emission from interstellar O VI has been convincingly detected more recently, with a doublet intensity of $\sim 3000 - 5000 \text{ LU}$ toward about a

dozen targets, using long (20-200 ksec) *FUSE* observations of $30''$ fields (Dixon et al. 2001; Welsh et al. 2002; Shelton et al. 2001; Otte et al. 2003).

The *SPEAR* mission was specifically designed to provide a spectral imaging survey of diffuse FUV emission from the ISM. We report the detection of such emission from most of the sky (see Figure 1). These data provide the first extensive spectral observations of FUV cosmic diffuse emission. We have found diffuse FUV emission lines emanating from both atomic and molecular species in a variety of interstellar environments.

3. THE SPEAR MISSION, OPERATIONS & DATA

SPEAR, aboard the S-1 satellite, was injected into a 700 km sun-synchronous orbit at 98.2° inclination with an orbital period of 98.5 minute and a ~ 34 minute eclipse. Observations are scheduled to begin ~ 360 s after eclipse entry and end ~ 300 s before eclipse exit. About 10 daily orbits are scheduled for astronomy observations. One or two orbits per day are used for down-looking observations of the northern night-side aurora. The 3-axis controlled spacecraft platform can use a star tracker to achieve $5'$ pointing knowledge, pointed accuracy of $\sim 6'$, and a stability of $\sim 12'$.

Various pointing modes are used for survey, target and calibration observations. Sky survey observations are performed by rotating a spacecraft axis such that the *SPEAR* field of view is swept, in a “push broom” fashion, perpendicular to its long field of view and in a 180° great circle from the north to south ecliptic pole via the anti-Sun direction. Following the anti-Sun progression in this way over one year would cause a full viewing of the sky with a maximum of overlapped exposure at the ecliptic poles and a minimum of exposure at the ecliptic plane. Calibration observations of stars or small ($\lesssim 10^\circ$) fields are performed by a “back and forth” spacecraft rotation that sweeps the field of view over a limited angle. The calibration pointing mode, together with reports of the spacecraft roll rate and the view-field’s ground-measured width, provide the most accurate positional data and exposure times for the observation of point sources. Fixed inertial pointing toward specific targets can also be performed. Pointings avoid the Sun by 45° , the spacecraft velocity vector by 60° and are limited to zenith angles of $< 110^\circ$.

The SaTReC Mission Operations Center, Daejeon, Korea is used to control the mission and receive data. Data are decommutated into spacecraft-time marked attitude and *SPEAR*-time marked science and engineering information. The information is passed through a photon reduction processing pipeline (Edelstein et al. *ibid*) that performs (1) engineering selection of valid photon events, (2) correction of detector electronic drift, (3) transformation from detector to physical coordinates, (4) correction of detector distortions, and (5) marking of photons with Universal time. A mission data processing pipeline creates (1) a time history of attitude knowledge, (2) a *SPEAR* to spacecraft time association history, (3) a time-associated sky exposure history and (4) photon lists with time-associated attitude information. The mission data products, in concordance with the photon data products, can then be combined to produce fluxed spectra and spectral sky maps.

Each photon event is mapped to the sky by using a

¹ Line intensity units, “LU”, are photons $\text{s}^{-1} \text{ cm}^{-2} \text{ sr}^{-1}$. Continuum intensity units, “CU”, are $\text{LU} \text{ \AA}^{-1}$.

combination of the spacecraft attitude information, the instrument's bore-sight offset from the spacecraft axis, and the angular position of the event on the detector. Absolute bore-sight is determined by correlating reconstructed sky images with a field of known bright stars. The spacecraft attitude knowledge, scheduled for report at 1-2 s intervals, is determined by a star-tracker and a gyroscope (gyro). The tracker updates are designed to set the gyro knowledge to $\sim 2'$ accuracy every 5 s. The gyro knowledge drifts at $0.2' \text{ s}^{-1}$. The knowledge error, derived from the drift rate and tracker update history, is assigned by the pipe-line processing for each photon. The sky location at times in-between spacecraft attitude reports is computed using a spherical coordinate interpolation.

Sky exposure is derived according to valid exposure intervals (typically 60 s) that are determined by examining operational and telemetry-interruption markers rks interleaved with the photon data. Time-marked exposure records are produced every 1.0 s within valid intervals for each $5'$ increment within the spectrometers' field-viewing angles. Each exposure event can then be mapped to a sky position in a similar fashion as for photons. Exposure events include a weighting factor to account for fractional-second intervals that may occur at the end of valid periods, for partial coverage of a sky pixel, or for other effects such as processing dead-time or angular vignetting (see Edelstein *ibid*). Time synchronization between the instrument and the spacecraft is based upon an interpolation between spacecraft time reports and a correction that uses precise, synchronized 1.0 Hz and 10 Hz timing marks which have been interleaved with the instrument data stream. The timing correction requires careful handling of clock interruptions or erroneous telemetry. Photon events are marked to a precision of 0.1 Hz with an estimated timing accuracy of 0.25 s. Events with indeterminate time synchronization or shutter position, usually due to corrupted and missing telemetry, are eliminated and correspond to a $\sim 2\%$ of the data.

3.1. Mission Performance

SPEAR's observational performance depends on sky coverage, sky exposure and mapping accuracy. We report on the first year's (2003 November – 2004 November) observations. The S-1 mission was designed for a 2-year mission, however spacecraft engineering problems may preclude further science observations. During the first year, 2450 orbits of observations were recorded. The S-1 attitude control system behavior limits the quality of attitude knowledge reconstruction. We find that the bore-sight offset is not constant on a per orbit basis due to a variation in the reporting of attitude. Furthermore, the star tracker updates are sometimes lost, resulting in an attitude error caused by gyro drift. Finally, especially toward the end of the year, star tracker updates or attitude knowledge reports are less frequently available. About 40% of our data suffer from some form of these problems.

The precision of attitude reconstruction from multiple, overlapping sky viewings is affected by the attitude system's stability. We have developed a systematic approach that uses *SPEAR* itself as a star tracker to correct for bore-sight variability in survey and calibration

sweeps. This method has been applied to the observation of individual targets and to ~ 850 survey sweep orbits. For observations that cycle sweeps over one field, the attitude timing delay is varied until L-band stellar images converge. Absolute bore-sight is then determined by using a 2-d correlation of the image to bright stars listed in the TD-1 catalog (Carnochan & Wilson 1983). For survey or other single sweep observations, a similar correlation is used between TD-1 catalog objects and the L-band sweep image, recomputed for variable timing delays. A single star's image can be reconstructed from multiple viewings to an effective resolution of $10'$ FWHM with a $10'$ positional accuracy. Survey sweep positional corrections in the sweep track direction are found to be $\pm 30'$ (2σ) and $\pm 8'$ (3σ) in the cross track direction. Because the S-1 attitude follows a time sequenced command program, *SPEAR* can produce an image of a sweep-observed region even when attitude knowledge is compromised or absent. We anticipate that the attitude correction for a large fraction of the data with yet-uncorrected attitude problems can be improved.

4. THE DIFFUSE FUV SKY: DATA REDUCTION

We derive a spectral sky-map of diffuse emission from these data, from which we introduce the appearance of the FUV sky and its total spectrum. Spectral sky maps were created by binning photon and exposure events using the HEALPix tessellation scheme (Górski et al. 2005) with $\sim 15'$ pixels and λ bins for the L and S bands of 1.0Å and 1.5Å, respectively. The accumulations, made only for times when the derived attitude error is $\leq 30'$, contains 1.2×10^7 and 1.4×10^7 photons for the L and S bands, respectively. The corresponding sky exposure map for the L-band, shown in Figure 1, covers $\sim 80\%$ of the sky and includes features such as deep exposures (>10 ksec) toward calibration and pointed study fields, and exposures of $>500 \text{ s degree}^{-2}$ near the north ecliptic pole where many survey sweeps overlap. Apparent are regions where no coverage exists due to the aforementioned attitude problems, to operational interruptions, and to detector-protective shutdowns while observing FUV intense regions such as the Galactic plane. The integrated exposure for the instantaneous field of view is 987 ks, with an average of 65 s degree^{-2} for observed sky regions. About 15% of these observations were taken using the 10% shutter aperture. The S-band exposure map is similar to the L-band map, although coverage is reduced due to the smaller field of view.

In order to obtain true images of the cosmic FUV sky, these data were subject to further reduction to account for artifacts, evident when simply dividing the photon map by the exposure map, and to account for detector background noise contribution. We proceed with artifact removal and analysis of the *SPEAR* L-band map, for 100% shutter-position observations, because of their superior coverage and sensitivity in comparison to the S-band data. The artifacts, e.g. streaking in the direction of survey sweeps and localized over-intense regions, are due to systematic errors in exposure determination and to the recording of data during times of high airglow or radiation background contamination. Over-intense regions due to erroneous mapping were eliminated by only including orbits that contain exposure records and photons that map to $>95\%$ of the identical sky pixels. Or-

bits having excessive airglow or particle induced detector noise were identified by using the H Lyman- β λ 1027 and O I λ 1356 count rates as airglow monitors. Entire orbits with an average Lyman- β rate exceeding 5 s^{-1} were eliminated. For certain regions showing residual ecliptic streaking that have been observed repeatedly using successive sweeps, entire orbits were rejected when their average monitor rate exceeded twice the dispersion of all the orbital rates about their median. The L-band spectral map, after artifact removal, contains 7.2×10^6 photons and 810 ks of full-field exposure.

To obtain the *diffuse* cosmic background, we attempt to remove bright concentrated sources, e.g. resolved stars, from the map. Because the FUV diffuse intensity varies by orders of magnitude across the sky, stars must be identified as *locally* intense pixels. An L-band total intensity map, integrated over $\lambda\lambda$ 1360 – 1710, was adaptively binned by sky area to attain a statistical signal to noise (S/N) ≥ 45 , value for each bin. In this scheme, the sky-bin size is increased along HEALPix pixel boundaries, i.e. for contiguous pixel groupings of size 4^n , until sufficient counts exist within the bin. In this way, bright objects retain small angular dimensions while faint regions are averaged to larger angular dimensions with values of improved significance. Bright sources were identified in $\sim 3\%$ of the pixels as having an intensity that exceeds 2.5 times the median value of the enveloping $4^\circ \times 4^\circ$ region (256 HEALPix bins). (We did not attempt to identify stars using point-spread function detection schemes in this preliminary work because, at each point in the sky, the mapped point-spread function is a composite of the elliptical instrumental spread-function whose orientation differs for each sweep direction.)

The first Galactic map of total diffuse *SPEAR* L-band FUV flux, shown in Figure 2, is obtained as an end product of the data reduction by eliminating the locally intense pixels from the starting continuum map, followed by adaptively binning the pixels to S/N ≥ 10 .

5. THE FUV SKY BRIGHTNESS & SPECTRA

The diffuse FUV L-band sky map (Figure 2) shows the largest intensity toward the Galactic plane and other regions where bright early type stars co-exist with significant columns of interstellar dust, such as the obvious features of the Sco-Cen association and the Magellanic Clouds. Thus, the cosmic FUV flux distribution is consistent with what is generally believed to be its dominant component, starlight scattered by interstellar dust (Bowyer 1991), and is therefore similar to maps of reddening, N(HI) and H- α (Schlegel et al. 1998; Dickey & Lockman 1990; Finkbeiner 2003) because both of these maps trace in some way either interstellar dust or the strong (local) FUV radiation fields that are required to produce the dust-scattered FUV continuum.

Far UV spectra of the sky are obtained by spatially binning the *SPEAR* L-band spectral sky-map. The integrated *faint-sky* (bright-star subtracted) and *bright-sky* (star-only) FUV spectra are shown in Figure 3, together with example spectra for the type of stars expected to dominate the direct and scattered stellar FUV background (Henry 2002). The *bright-sky* spectrum has a $\lambda\lambda$ 1360 - 1710 median intensity of $\sim 30\text{k}$ CU. The *faint-sky* diffuse spectrum has a band median intensity of 2.3k CU that includes contributions from a true cosmic sig-

nal, a combination of direct unresolved and interstellar dust-scattered starlight, and residual instrumental background.

The spectral fitting model of Korpela et al. (*ibid*) is used to identify and estimate the strength of both the astronomical and instrumental components within the *faint-sky* signal. We find a median detector dark-noise contribution of 460 CU, the geo-coronal emission line, O I λ 1356, and a number of prominent spectral features which we identify as diffuse astrophysical emission lines from the ISM. Strong emission lines from abundant interstellar species in this bandpass can typically be identified with confidence because they are usually well separated from each other and from night-time geocoronal lines, although features from unresolved stars or scattered starlight and from interstellar H₂ do add some confusion to the spectrum. Line identifications and intensities of prominent features are shown in Table 1, along with the intensities' statistical error (10 - 20 %) and line-fit modeling error.

Lines found that are likely to originate from the warm/hot ISM include the pronounced C IV $\lambda\lambda$ 1549 feature and the O IV] / Si IV $\lambda\lambda$ 1400/1403 blend, previously detected and tentatively identified, respectively, by Martin & Bowyer (1990) at similar intensities. Interstellar diffuse lines, newly discovered with *SPEAR*, include the Si II* λ 1533 and Al II λ 1672 resonance lines that could originate from either neutral or warm ionized ISM. We attribute the bright 1533 Å feature to the Si II* λ fine structure ground state transition given that the Si II λ 1527 ground state transition should be optically thick for typical interstellar conditions and therefore undetectable. The Al II λ 1671 feature may have been misidentified as the O III] $\lambda\lambda$ 1665 doublet in prior lower resolution observations (Martin & Bowyer 1990). Also discovered with *SPEAR* is diffuse 1657 Å emission from C I, a species that exists in the ISM despite photoionization by the FUV background (Jenkins & Tripp 2001).

The FUV H₂ fluorescence emission, previously detected by Martin et al. (1990), presents prominent and recognizable features in the *faint-sky* spectra (Black & van Dishoeck 1987), particularly at λ 1608 and λ 1580. (See the *SPEAR* observations of H₂ in Eridanus by Ryu et al. *ibid*, for examples of the H₂ fluorescence spectral signature and band identification.) We identify the feature at 1639.1 Å as He II λ 1640 diffuse emission, although the fit line width, 50% larger than other identified features, indicates spectral contamination from H₂ or from O I airglow, although the night-time only observations mitigates potential O I contamination. Some spectral features appear in both the *bright-sky* and the *faint-sky* spectra, such as those at λ 1485 and λ 1520, which we tentatively attribute to residual stellar features and some possible contribution from the H₂ fluorescence bands. The total intensity estimated for all of the prominent interstellar atomic spectral lines is $\sim 10\text{k}$ LU, and for the distinct H₂ fluorescence bands is $\sim 9\text{k}$ LU.

6. *SPEAR* RESULTS

These FUV continuum and emission line data contain much astrophysical information. The continuum distribution depends upon the interstellar dust and radiation field, the H₂ fluorescence reveals the molecular distribu-

tion and destruction rate, and the FUV emission lines indicate the ionization equilibrium state and energetics of the ISM. We shall explore these matters in future publications and present *SPEAR* spectral-line sky maps, work which requires comprehensive analyses that is beyond the scope of this introductory letter. We refer the reader to accompanying papers following in this volume, summarized below, that use *SPEAR* data and provide detailed discussions on the identification and importance of the FUV spectral components in different interstellar environments.

6.1. The Diffuse ISM

Korpela et al (*ibid*) present *SPEAR* S and L-band spectra of the North Ecliptic Pole (NEP) region ($\beta = +30^\circ$, $N(\text{HI}) 2\text{--}8 \times 10^{20} \text{ cm}^{-2}$), a region that has no obvious associations with active interstellar regions and therefore represents a canonical sight-line through the ISM. A large number of diffuse FUV atomic emission lines are detected in the NEP, representing the warm neutral to the hot ionized medium. The atomic lines, ranging from 1500 to 6000 LU in intensity, include those identified in the L-band all-sky spectrum previously presented, as well as O VI, C III, N II in the S-band, and N IV] in the L-band. Presuming that the resonance lines are not dominated by scattering of the interstellar radiation field, it is found that the high ionization potential lines cannot be fit by a collisional ionization equilibrium plasma model even though these lines, modeled on a per species basis, have consistent emission measures, 0.001 to $0.005 \text{ cm}^{-6} \text{ pc}$, over the $10^{4.5}$ to $10^{5.5}$ K temperature range. Therefore, it appears that photo-excitation, non-equilibrium effects or abundance variations are important in any explanation of the spectrum. In addition, substantial H₂ fluorescence emission is detected in the NEP, despite the region's moderately low N(HI).

6.2. FUV Hydrogen Fluorescence & Continuum

SPEAR observations show that interstellar FUV H₂ fluorescence is ubiquitous, consistent with FUV absorption observations (Shull et al. 2000; Gillmon et al. 2005) that find H₂ over large portions of the sky. Lee et al. (*ibid*) observes H₂ fluorescence in the Taurus cloud's halo but not from the dense cloud core, a fact attributed to the core's opacity excluding the FUV radiation needed to induce fluorescence. Ryu et al. (*ibid*) finds H₂ fluorescence emission over a large region about the Ori-Eri super-bubble and is able to elucidate the geometry of the Ori-Eri region by comparing the FUV fluorescence with H _{α} and reddening maps and models an H₂ excitation temperature of ≥ 1000 K, larger than generally found for molecular gas in the Galactic disk. The H₂ fluorescence is also found in deep *SPEAR* observations of the Ori-Eri super-bubble interface to the ambient ISM (Kregenow et al. *ibid*).

The *SPEAR* observation of the Taurus cloud (Lee et al, *ibid*) shows a counter-intuitive anti-correlation of FUV continuum with visual extinction and IR dust emission. The FUV continuum map of Taurus provides an optical transfer relation over a wide range of depths that can be used to quantify the dust and illumination properties – the cloud core appears to block more distant FUV

flux while the cloud halo scatters local flux toward the observer.

6.3. Supernova Remnants and Superbubbles

SPEAR data provide unique spectral images of two nearby and well studied SNRs, Vela SNR (Nishikida et al *ibid*) and the Cygnus Loop SNR (Seon et al *ibid*). Both authors find that the spatial distribution of FUV emission cannot be simply predicted using visible H _{α} or X-ray emission maps. The remnants' emission line images, recorded in C III, O III], C IV and O VI far UV lines, show where radiative shocks with velocities ranging from ~ 100 - 200 km s^{-1} prevail. The work directly verifies that the FUV emission lines are important to SNR cooling. For Vela, the combined luminosity of strong FUV lines exceeds the 1.0 – 4.0 keV X-ray luminosity by an order of magnitude, with a FUV to X-ray flux ratio that is a few times larger than that for the Cygnus Loop. The Vela enhancement is attributed in part to its higher covering factor of relatively dense material that can give rise to FUV bright shocks.

Kregenow et al. (*ibid*) reports on *SPEAR* spectra imaged across the shell-wall boundary surrounding the Ori-Eri superbubble, an X-ray emitting interstellar cavity that may have been created by SNR or stellar winds. The FUV spectra are rich and include lines of similar species and intensities as found in the all-sky spectrum and in the NEP (Korpela et al. *ibid*). Kregenow's study discovers a distinct correspondence of O VI, C IV, and Si II* with the shell-wall interface traced in H _{α} , an unprecedented diagnostic for this type of evolved structure. The work finds that the boundary emission is may be explained by either a quiescent thermal interface or a shocked region.

7. CONCLUSION

The first FUV spectral imaging survey of the large fractions of the sky has been taken with the *SPEAR* mission. The resulting map of total FUV radiation shows that diffuse FUV cosmic radiation is concentrated where both hot stars and scattering dust coexist, such as in the Galactic plane, young stellar associations, and the Magellanic clouds. The spectra of the total-sky contains prominent lines from ionized gas, including the previously observed C IV and Si IV emission, and from newly discovered C I, Si II*, Al II, He II emission, as well as from H₂ fluorescence. Similar interstellar FUV emission lines are found in the general ISM, as sampled at the NEP, and toward the Eri-Ori superbubble and its interface to the ISM. Intense FUV emission lines from shocks are visible in nearby SNR. Diffuse H₂ fluorescence is ubiquitous across observed Galactic environments. Much work remains to elaborate upon the character of the FUV sky and to analyze the physical conditions of detailed objects.

SPEAR / *FIMS* is a joint project of KASI & KAIST (Korea) and U.C., Berkeley (USA), funded by the Korea MOST and NASA Grant NAG5-5355. We thank the team for their remarkable effort to create the mission and families and friends for their love and support. Thanks Phil.

REFERENCES

- Black, J. H. & van Dishoeck, E. F. 1987, *ApJ*, 322, 412
- Borkowski, K. J., Balbus, S. A., & Fristrom, C. C. 1990, *ApJ*, 355, 501
- Bowyer, S. 1991, *ARA&A*, 29, 59
- Carnochan, D. J. & Wilson, R. 1983, *MNRAS*, 202, 317
- Davidsen, A. F. 1993, *Science*, 259, 327
- Dickey, J. M. & Lockman, F. J. 1990, *ARA&A*, 28, 215
- Dixon, W. V. D., Sallmen, S., Hurwitz, M., & Lieu, R. 2001, *ApJ*, 552, L69
- Edelstein, J. et al. 2005, *ApJ*, this issue
- Finkbeiner, D. P. 2003, *ApJS*, 146, 407
- Gillmon, K., Shull, J. M., Tumlinson, J., & Danforth, C. 2005, *apJ*, submitted
- Górski, K. M., Hivon, E., Banday, A. J., Wandelt, B. D., Hansen, F. K., Reinecke, M., & Bartelmann, M. 2005, *ApJ*, 622, 759
- Henry, R. C. 2002, *ApJ*, 570, 697
- Hurwitz, M., Bowyer, S., Kudritzki, R.-P., & Lennon, D. J. 1995, *ApJ*, 450, 149
- Hurwitz, M., Sasseen, T. P., & Sirk, M. M. 2005, *ApJ*, 623, 911
- Jenkins, E. B. 1978, *ApJ*, 219, 845
- Jenkins, E. B. & Tripp, T. M. 2001, *ApJS*, 137, 297
- Korpela, E. J. et al. 2005, *ApJ*, this issue
- Kregenow, J. et al. 2005, *ApJ*, this issue
- Lallement, R. 2004, *A&A*, 422, 391
- Landini, M. & Monsignori Fossi, B. C. 1990, *A&AS*, 82, 229
- Lee, D.-H. et al. 2005, *ApJ*, this issue
- Martin, C. & Bowyer, S. 1990, *ApJ*, 350, 242
- Martin, C., Hurwitz, M., & Bowyer, S. 1990, *ApJ*, 354, 220
- Martin, D. C. et al. 2005, *ApJ*, 619, L1
- McCammon, D. et al. 2002, *ApJ*, 576, 188
- McKee, C. F. 1995, in *ASP Conf. Ser. 80: The Physics of the Interstellar Medium and Intergalactic Medium*, 292+
- Nishikida, K. et al. 2005, *ApJ*, this issue
- Otte, B., Dixon, W. V., & Sankrit, R. 2003, *ApJ*, 586, L53
- Ryu, K.-S. et al. 2005, *ApJ*, this issue
- Sanders, W. T., Edgar, R. J., Kraushaar, W. L., McCammon, D., & Morgenthaler, J. P. 2001, *ApJ*, 554, 694
- Savage, B. D., Sembach, K. R., Wakker, B. P., et al. 2003, *ApJS*, 146, 125
- Schlegel, D. J., Finkbeiner, D. P., & Davis, M. 1998, *ApJ*, 500, 525
- Sembach, K. R. & Savage, B. D. 1992, *ApJS*, 83, 147
- Seon, K.-I. et al. 2005, *ApJ*, this issue
- Shapiro, P. R. & Benjamin, R. A. 1991, *PASP*, 103, 923
- Shelton, R. L. 1998, *ApJ*, 504, 785
- Shelton, R. L., Kruk, J. W., Murphy, E. M., et al. 2001, *ApJ*, 560, 730
- Shinn, J.-H. et al. 2005, *ApJ*, this issue
- Shull, J. M. & Slavin, J. D. 1994, *ApJ*, 427, 784
- Shull, J. M. et al. 2000, *ApJ*, 538, L73
- Slavin, J. D. & Cox, D. P. 1992, *ApJ*, 392, 131
- . 1993, *ApJ*, 417, 187
- Snowden, S. L., Egger, R., Finkbeiner, D. P., Freyberg, M. J., & Plucinsky, P. P. 1998, *ApJ*, 493, 715
- Wargelin, B. J., Markevitch, M., Juda, M., et al. 2004, *ApJ*, 607, 596
- Welsh, B. Y., Sallmen, S., Sfeir, D., et al. 2002, *A&A*, 394, 691
- Zsargó, J., Sembach, K. R., Howk, J. C., et al. 2003, *ApJ*, 586, 1019

TABLE 1
IDENTIFICATION OF *faint-sky* LINE FEATURES

Species	λ	λ_{fit}	I_λ	Statistical Error	Model Uncertainty
	Å	Å	LU ^a	LU	LU
Si IV ^c	1403	1403.1	736	162	281
Si II*	1533	1532.0	1909	201	275
C IV	1550	1548.7	2636	211	341
H ₂	1608	1606.5	1832	262	385
He II	1640	1639.1	3577	378	1177
C I	1657	1655.7	1316	276	487
Al II	1670	1669.7	1474	280	226

^aLU=ph s⁻¹ cm⁻² sr⁻¹

^bLU=ph s⁻¹ cm⁻² sr⁻¹

^cblended with OIV] 1400

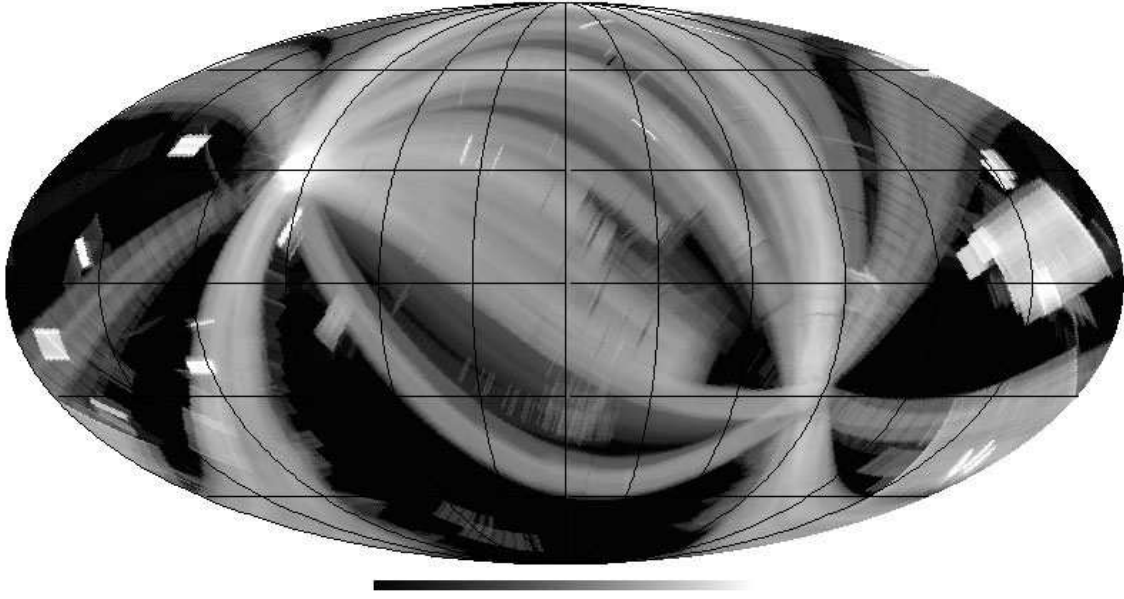


FIG. 1.— Sky exposure for the *SPEAR* L-band observations. The map is made with 0.5° pixels, a histogram equalized intensity scale with a maximum of $500 \text{ s degree}^{-2}$, Galactic Aitoff coordinates centered at $l, b = 0^\circ, 0^\circ$ with longitude increasing toward the left, and is shown with latitude and longitude lines on a 30° grid.

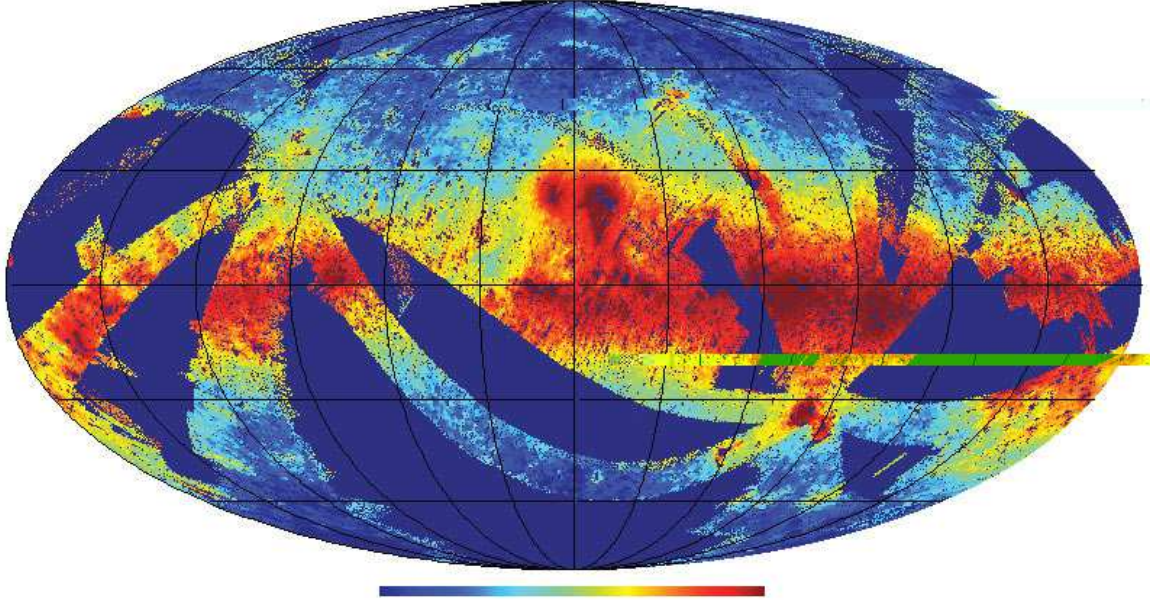


FIG. 2.— T

total diffuse intensity map of the sky for the *SPEAR* L-band ($\lambda\lambda$ 1360 - 1730) observations, after removal of locally intense pixels (stars). The map, in the same coordinates scheme as Figure 1, has a histogram equalized logarithmic intensity scale with a maximum of 20k CU, and is adaptively binned by sky area to a $S/N \geq 10$. Evident features include the Galactic Plane, the Sco-Cen association (e.g. zeta-Oph at $l, b = 6^\circ, 24^\circ$), and the LMC at $l, b = 280^\circ, -32^\circ$.

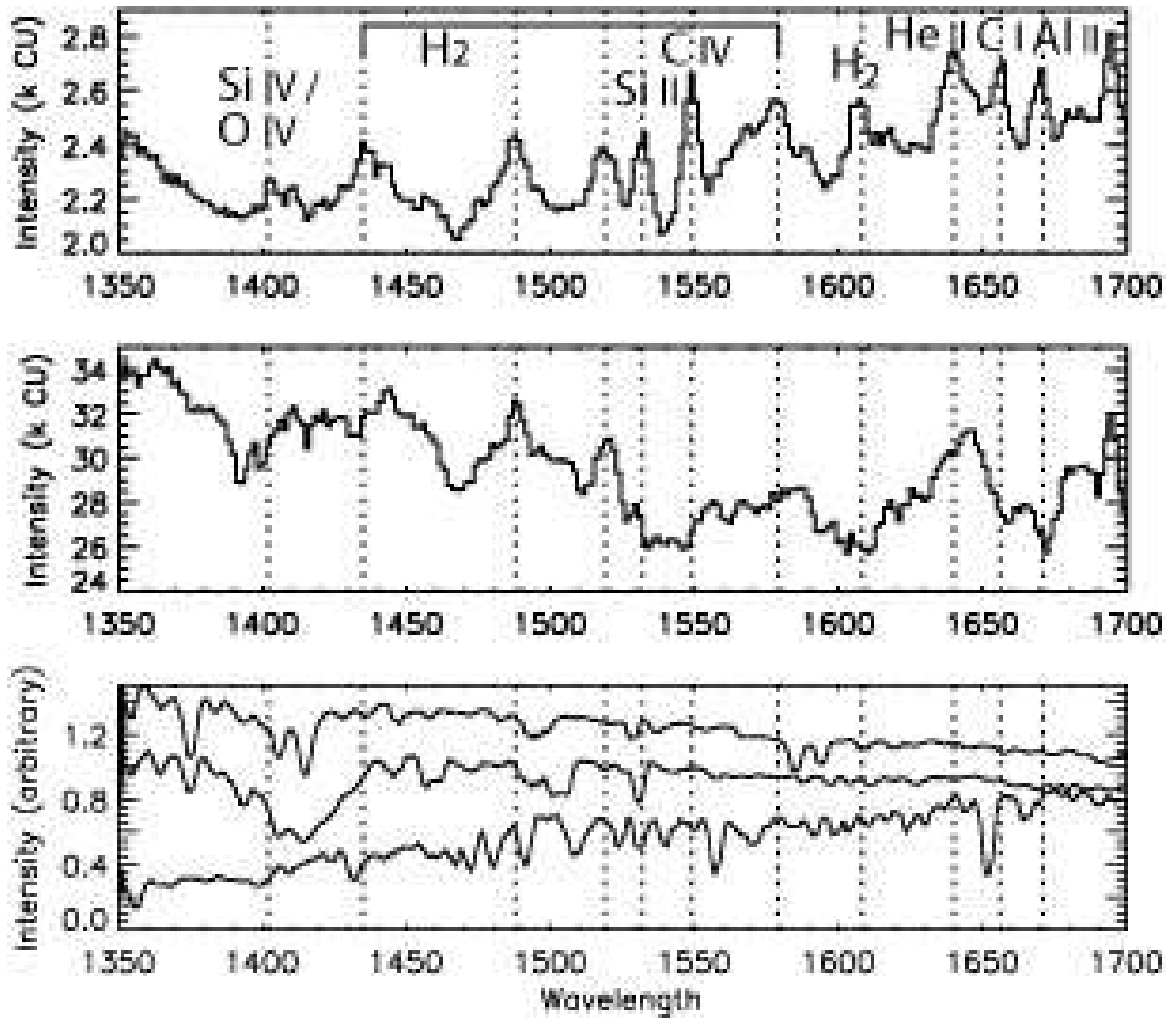


FIG. 3.— The L-band spectra (*top*) from the *faint-sky* and (*middle*) from the *bright-sky*, plotted with false zeros. (*bottom*) IUE measured stellar spectral for B3V, B5V and B8V stars in arbitrary units. Dashed lines mark prominent *faint-sky* spectral features.